12

MAGNETIC SHIELDING

V. V. Yashchuk, S.-K. Lee, and E. Paperno

12.1 Introduction

The ability to obtain well characterized, stable magnetic field conditions independent of the Earth's magnetic field ($\sim 0.3-0.6$ G) and environmental perturbations is the key to many urgent fundamental and applied investigations using high-precision magnetometry.

State-of-the-art magnetometers operate with a sensitivity on the level of $1-10\times 10^{-12}$ G/$\sqrt{\text{Hz}}$ (see Chapters 4-10), whereas the amplitude spectrum of geomagnetic noise (see, for example, Ref. [1]) varies from about 0.2 G/$\sqrt{\text{Hz}}$ at 10^{-5} Hz (about a day observational period) to 2×10^{-8} G/$\sqrt{\text{Hz}}$ at 1 Hz (about a second observational period) with an approximately inverse-power-law (fractal-type) frequency dependence, scaled as $f^{-1.4}$ [1]. In order to provide the required stability of the magnetic field, different techniques of magnetic shielding and stabilization have been brought into practice.

Despite the considerable amount of literature on experiments vitally dependent on the efficacy of magnetic shielding, the details of the design of shielding systems and their performance are scarce and, until now, scattered among numerous publications.

In this chapter, we review the physical principles of magnetic shielding and discuss design approaches, performance characterization, and the use of shielding systems. We begin in Sec. 12.2 with a discussion of fundamentals and basic approaches to designing and optimally using a ferromagnetic shield. Peculiarities of ferrite-based and superconducting shields are considered in Sec. 12.3 and Sec. 12.4, respectively.

12.2 Ferromagnetic shielding

Depending on the frequency of external magnetic fields, ferromagnetic shielding occurs through different physical mechanisms. For static and low-frequency fields, the most important mechanism is flux shunting due to a high magnetic permeability, μ, of the material (see, for example, reviews [2, 3, 4, 5, 6]).

At higher frequencies, the skin effect starts to play an essential role becoming predominant at frequencies $\geq 10 - 50$ Hz for rather thick (thickness $t \geq 1$ mm) shielding shells made of high permeability ($\mu \geq 10^5$) materials. Practically, a ferromagnetic shield optimized for shielding static fields automatically provides efficient shielding of oscillating fields. Therefore, we concentrate the discussion on the case of static and low-frequency fields. Shielding in the intermediate-frequency regime where both mechanisms are equally important is discussed, for example, by Hoburg [7].

12.2.1 Simplified estimation of ferromagnetic shielding efficiency for a static magnetic field

To shield a space, the external magnetic flux is directed around it via a high-permeability ferromagnetic material [Fig. 12.1(a)]. The efficiency of a shield can be characterized by the shielding ratio

$$T \equiv \frac{B_{in}}{B_0} \ , \tag{12.1}$$

where B_0 is the homogeneous magnetic field existing before introducing the shield, and B_{in} is the field induced inside the shield due to B_0.

We should note here that in the literature there are different definitions of the shielding efficiency (ratio, factor). Here, we use the terminology of Ref. [3] where of the shielding efficiency (ratio) is defined as in Eq. (12.1).

According to Rowland's law (Ohm's law for magnetic circuits) [8, 9], for static fields the shielding efficiency depends on the relation of the effective resistances (reluctances) of the ferromagnetic "yoke," $R_f = L_f/\mu S_f$, and that of the inner space, $R_s = L_s/S_s$ [see Fig. 12.1(a)], where L_i is the characteristic length and S_i is the cross-section of the corresponding magnetic circuit (see, for example, [6, 10, 11]). These magnetic reluctances constitute a divider for the magnetic flux $\Phi_o = B_o S_o$ dividing it into Φ_{in} and Φ_f:

$$\frac{\Phi_{in}}{\Phi_f} = \frac{R_f}{R_s} \ . \tag{12.2}$$

The resulting shielding ratio for a single ferromagnetic shell shown in Fig. 12.1(a) can be estimated supposing $L_f \approx L_s \approx X$, $S_o \approx S_s$, $S_s \propto X^2$, and $S_f \propto tX$:

$$T_a = \frac{\Phi_{in} S_o}{\Phi_o S_s} \approx \frac{\Phi_{in}}{\Phi_f + \Phi_{in}} \approx \frac{R_f/R_s}{1 + R_f/R_s} \propto \frac{\frac{X}{\mu t}}{1 + \frac{X}{\mu t}} \approx \frac{X}{\mu t} \ , \tag{12.3}$$

where X is the characteristic size of the shell, such that $\mu t \gg X$.

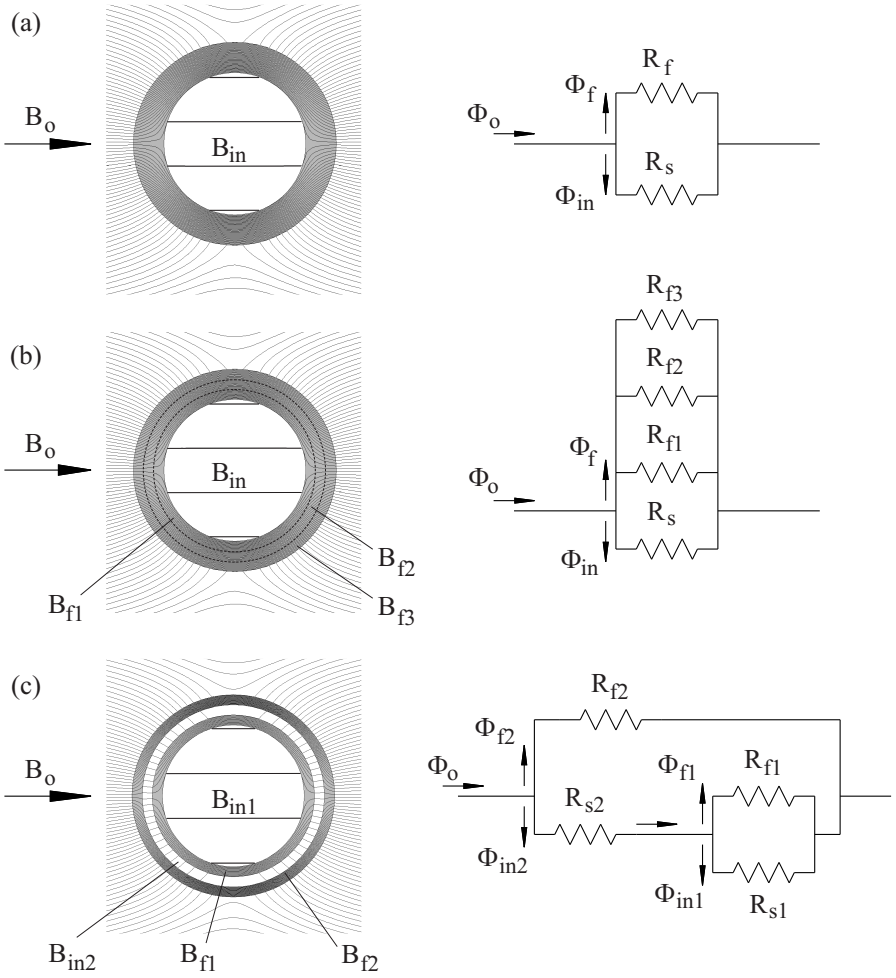

Figure 12.1 Magnetic circuit approach to estimating the performance of a multilayer shield.

12.2.2 Multi-layer ferromagnetic shielding

According to Eq. (12.3), a way to improve shielding efficiency is to increase the shell thickness t as illustrated in Fig. 12.1(b), where the thick cylindrical shield is divided into three equal thickness shells. Being perfectly coupled, these three shells can be thought of as a circuit of reluctances connected in parallel and conducting nearly the same flux. It gives

$$T_b \propto \frac{X}{\mu(t_1 + t_2 + t_3)} \ , \tag{12.4}$$

supposing $X \gg t_i$.

However, a much more efficient way to improve shielding efficiency is to use multi-layer shielding as shown in Fig. 12.1(c). In this case, the equivalent magnetic circuit consists of two dividers providing an overall shielding ratio proportional to the product of the shielding ratios of the separate shells:

$$T_c = \frac{\Phi_{in1} S_o}{\Phi_o S_{s1}} \approx \frac{\Phi_{in}}{\Phi_{in} + \Phi_{f2}} \frac{\Phi_{in1}}{\Phi_{in1} + \Phi_{f1}} \propto \frac{X_1}{\mu_1 t_1} \frac{X_2}{\mu_2 t_2} \ , \tag{12.5}$$

Here, for simplicity, we use the assumptions that $S_o \approx S_{s1} \approx S_{s2}$ and that the gap between the layers is on the order of X_2.

Efficiency of the multi-layer design can be illustrated on an example of the particular shielding geometry depicted in Fig. 12.1. For this case and assuming $\mu = 60$, numerical simulation using ANSYS Maxwell 13 software [12] shows that the same shielding efficiency is obtained with a thick single shell [Fig. 12.1(a)] and with two thinner nested shells with a significantly lower total weight [Fig. 12.1(c)]. For a higher μ, shielding with two separated layers appears to be even larger than that of the single shell.

Thus, introducing air gaps between the shells can help maintain the same shielding efficiency despite removing a significant part of the shielding material. Simply put: it is worth shielding the shielding shells.

Effect of shell shape

The advantage of using multi-layer shielding was demonstrated both experimentally and theoretically as far back as the end of the 19$^{\text{th}}$ century [13, 14, 15, 16]. In the course of the 20$^{\text{th}}$ century, a number of publications were devoted to the development of an analytical approach to derive simple formulae for the shielding efficiency for different geometries: cubic and cylindrical shields of finite length [2, 7, 17, 18, 19, 20], spherical and spheroidal shields [21, 22, 23, 24]. A systematic review of early works as well as a theoretical treatment and comparison with practical realizations can be found in the work of Sumner *et al.* [2]. The analysis of various shielding geometries and configurations is presented in detail in a book by Rikitake [3]. A comparison of the analytical expressions from Refs. [2, 18] for the axial-field shielding with the results of numerical calculations is given in Ref. [19], where analytical formulae for better approximation of the shielding efficiency for a multilayer cylindrical shield are also presented. Four-layer cylindrical shields with hemispherical and conical end caps are described in Ref. [25].

The dependence of the shielding efficiency on the shapes and sizes of shells of a multi-layer shield can be summarized by a simplified formula:

$$T_{tot} \equiv \frac{B_{in}}{B_0} \approx T_n \times \prod_{i=1}^{n-1} T_i \left[1 - \left(\frac{X_{i+1}}{X_i} \right)^k \right]^{-1} \ ; \ \ T_i \approx \frac{X_i}{\mu_i t_i} \ . \tag{12.6}$$

In Eq. (12.6), T_i is the shielding efficiency of a separate i-th shell, X_i ($X_i > X_{i+1}$) is the layer's radius or length (depending on the relative orientation of the magnetic

field and the layer), t_i and $\mu_i \gg X_i/t_i$ are the thickness and magnetic permeability, and n is the number of shells. Good approximations of the powers k are: $k = 3$ for a spherical shield, $k = 2$ and $k = 1$ for the transverse and axial shielding ratios of a cylindrical shield with flat lids, respectively.

Equation (12.6) shows that spherical shells provide the best shielding (for shields of comparable dimensions). Moreover, spherical shields provide a uniform field within the shielded area. (Note that infinitely-long cylindrical shields also possess this property.)

Unlike spherical shields, the shielding efficiency of cylindrical shields depends on the direction of the applied field. The axial shielding factor of closed cylindrical shields decreases with the shield length (i.e., the shielding improves as the length to diameter ratio increases). For a single-shell shield with equal length and diameter, it is 90% compared to the transverse shielding factor. Increasing the shield length decreases the axial shielding factor in approximately inverse proportion, for example, down to about 46% and 21% for the length increase by a factor of 2 and 4, respectively [19]. To obtain substantial axial shielding with open-ended cylindrical shields, their lengths should significantly exceed their diameters [19, 26]. It is important also to note that open-ended cylindrical shields with optimized length [19, 26] can provide better axial shielding, both in terms of the shielding ratio and the residual field homogeneity, than their closed counterparts with flat caps. A simplified explanation is that shielding caps "attract" an extra magnetic flux that leaks inside the shield. Note also that in the limit of infinitely long cylinders, either open or closed, axial shielding vanishes, approaching one.

Thus a spherical shield is preferable if one thinks of the equal shielding efficiency in all directions, the overall size, and cost of the material. The axial shielding efficiency of closed axial cylindrical shields can be improved by using conical caps (see Sec. 12.2.5).

Optimal shell separation

As shown above, a multilayer shield with thin shells and relatively wide gaps between them can be as effective as a much heavier and more expensive thick, single-layer shield. To minimize the total size of a multilayer shield, the air gaps between its shells should be optimized.

For two coaxial infinitely long cylinders with the same thickness t, relative permeability μ, and outer diameters D_1 and D_2, such that $D_1 > D_2$, the transverse shielding ratio for $T_i = D_i/(\mu t) \ll 1$ is approximately given by [27] [compare with Eq. (12.6)]:

$$T_{tot} = T_2^2 \frac{D_1}{D_2} \left(1 - \frac{D_2^2}{D_1^2}\right)^{-1} . \tag{12.7}$$

Straightforward differentiation of Eq. 12.7 suggests an optimal ratio of diameters of $D_1/D_2 = \sqrt{3}$. Assuming $D_2 \gg t$, the optimal gap, Δ_{opt}, for the double-shell

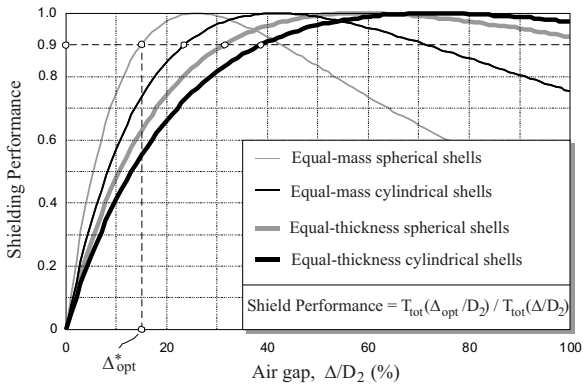

Figure 12.2 The effect of the relative air gap Δ/D_2 on the shielding performance of double-shell spherical and infinitely long cylindrical ferromagnetic shields. Equal-mass shields provide the most effective shielding per unit mass, but most practical shields are made using constant thickness material. (Adapted from Ref. [28].)

infinitely long cylindrical shield under consideration is $\Delta_{opt} \approx 0.73D_2$. Similar consideration for two concentric spherical shells gives the optimal ratio of the diameters of $D_1/D_2 = \sqrt[3]{4} \approx 1.59$ that corresponds to the optimal gap of $\Delta_{opt} \approx 0.59D_2$.

Figure 12.2 shows the shielding performance of double-shell spherical and infinitely long cylindrical ferromagnetic shields calculated assuming either equal mass or equal thickness of the shells [28]. For all the cases depicted in Fig. 12.2, the shielding performance, defined as the ratio of the shielding efficiencies for optimized and unoptimized size of the gap, rises quickly at first with increasing the gap and, after reaching the maximum at the optimal gap, gradually decreases.

Note that in Fig. 12.2, a 90% performance is reached at the gap significantly smaller than Δ_{opt}. For example, an equal-mass double-shell spherical shield would have 90% performance at $\Delta \approx 0.15D_2$; for a similar shield combined of long cylinders, $\Delta \approx 0.24D_2$. In a more practical case, where the shell thickness is kept constant, a double-shell spherical and a cylindrical shields with 90% performance would have $\Delta \approx 0.32D_2$ and $\Delta \approx 0.39D_2$, respectively. These gap values are significantly smaller than the exact optimal values found above.

Therefore from the point of view of shield cost and size, it is reasonable to define the optimal shell separation, Δ^*_{opt}, as the smallest gap that provides 90% of the maximum shielding performance. Separating shells with the Δ^*_{opt} gap rather than a gap that provides best shielding allows one to make the multilayer shield much more compact, without significantly sacrificing its shielding performance.

The optimal shell separation Δ^*_{opt} can be found analytically only for the simplest shielding assemblies, such as spherical and infinitely long cylindrical shields [27]. Multi-shell shields that are most widely used in practice have relatively short, closed cylindrical shells. Their shielding performance is typically limited by the axial shielding, so if effective shielding in all directions is desired, it is sufficient to optimize the shell separation focusing on the axial shielding efficiency.

Reference [28] shows that in contrast to spherical and infinitely long cylindrical shields, for equal-thickness closed axial cylindrical shields the optimal separation is surprisingly small. Depending on the shield geometry, Δ^*_{opt} varies between 5% and 17% of the inner shell diameter.

For practical purposes, the axial shielding with two closed cylindrical shells and relatively narrow air gaps can be estimated by using empirical formula [28]:

$$T_{tot} \approx 1.92\, T_2^2\, \alpha\, (1 + 0.1/\Delta_a + 0.06 \times \alpha^2/\Delta_r)\ , \tag{12.8}$$

where Δ_a and Δ_r are axial and radial air gaps relative to the inner shell diameter, D_2, and $\alpha = L_2/D_2$ is the aspect ratio of the inner shell.

Effect of openings

The design of a shield should usually provide access via multiple openings into the shielded area, for example, for laser beams, connecting wires of the inner coils, etc. Unfortunately, the openings also allow magnetic fields to penetrate inside the shield.

Magnetic field penetrating through an open end of a cylindrical shield decreases exponentially (Refs. [3, 18], for example):

$$B_{in} \approx B_0 e^{-\beta x/D}\ , \tag{12.9}$$

where B_{in} is either a transverse or longitudinal fringing field at the distance x from the shield end; the factor β equals about 7.0 and 4.5 for transverse and longitudinal fields, respectively; and D is the inner diameter of the shield. According to Eq. (12.9), at a distance of one diameter from the shield end, transverse and longitudinal fields are attenuated by factors of 10^3 and 10^2, respectively.

An opening in a shield with a diameter d much smaller than the characteristic sizes of the shield can be thought of as a removed magnetic dipole; so that the field from the opening should drop as x^{-3}. More accurate estimation of the components of an axial magnetic field penetrating through partial openings in the caps of a cylindrical shield can be obtained with a numerically verified empirical expression given in Ref. [29].

In order to reduce the effect of openings, one can widen the air gaps between the shielding shells [30]. The penetration of magnetic field can also be suppressed with cylindrical ferromagnetic collars mounted over the openings in the shells [31]; see also Sec. 12.2.5. Practically, at an aspect ratio of a collar of $l/d \approx 2 - 3$, the penetrating field becomes negligible.

Note that for alternating fields, openings can even enhance the shielding factor [32]. This is because the field penetrating through the shield walls has a phase shift with respect to the outside field; whereas the field coming in through the openings is in phase with the outside field (low frequencies). The phase difference of the fields depends on the shield design. At some frequency, it can become close to π, providing a resonance enhancement of the shielding factor. In Ref. [33] due to use

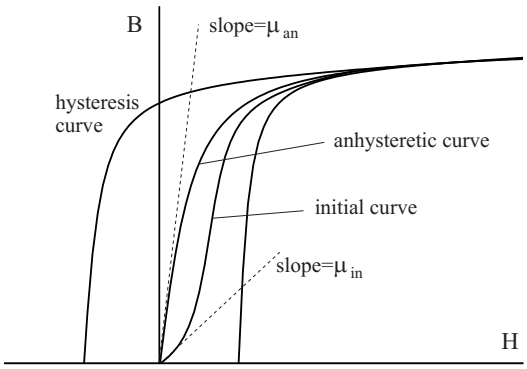

Figure 12.3 Hysteresis magnetization curve of a ferromagnetic material and various definitions of permeability.

of the phase-shift mechanism, an order of magnitude enhancement of the shielding factor at 22 Hz has been achieved.

12.2.3 Optimization of permeability: annealing, degaussing, shacking, tapping

Shielding efficiency strongly depends on the magnetic permeability of the shielding material [Eqs. (12.3) – (12.6)], which itself depends on the applied field and exhibits hysteretic behavior (see Fig. 12.3).

The best shielding is obtained well away from magnetic saturation of the shielding material. As shown in Fig. 12.1(c), magnetic flux density in multilayer shields is much higher in the outermost shell than in inner ones. Therefore, the outermost shell should be checked for saturation at the outset. For typical ferromagnetic shielding materials, such as Mumetal [34, 35], the maximum magnetic flux density should be below 2×10^3 G. In the Earth's field this implies requirements for the shield geometry of $D/t \leq 4000$ for transverse shielding and $L^3/tD^2 \leq 1.6 \times 10^7$ for axial shielding in the case of $2 \leq L/D \leq 40$ [2].

The magnetic permeability of the shielding material is also significantly affected by the treatment history of the material, its residual imperfections and stresses, as well as by handling and mounting.

Annealing

Imperfections and stresses in a shielding material, which obstruct the free motion of the magnetic domain boundaries, are significantly reduced by applying an appropriate annealing procedure. With high nickel content soft-ferromagnetic alloys, such as Mumetal [34, 35], Permalloy [36], and CO-NETIC [37], widely used for magnetic shielding, annealing in dry hydrogen atmosphere is strongly recommended as the final step in the fabrication process.

Hydrogen annealing provides multiple effects. The annealing removes impurities, such as carbon and sulphur, and alters the material's crystal structure by removing

stresses and aligning the grains (see, for example, Refs. [38, 39] and references therein). As a result, the material's permeability and shielding performance are significantly improved [40, 41, 42].

Martin and Snowdon [42] have investigated the magnetic shielding effect of CO-NETIC foil of a 0.1 mm thickness at a broad range of temperatures, from 4.2 K to 293 K. It was shown that annealed shields were an order of magnitude more effective at all temperatures.

If annealing is performed at zero magnetic field, the magnetization properties of the material are described by the initial magnetization curve [43, 44, 45] (Fig. 12.3). The slope of the curve at low magnetic fields gives an initial permeability, μ_{in}. For high-permeability materials, μ_{in} is typically smaller by an order of magnitude than the maximum permeability, μ_{max}. For example, for a perfectly annealed CO-NETIC AA alloy the initial permeability is specified to be $\mu_{in} = 30\ 000$, whereas $\mu_{max} = 450\ 000$ [46].

Degaussing

With a large shielding ratio, the main factor determining the residual magnetic field inside the shield is the residual magnetization of the innermost shielding layer. This residual magnetization is subject to change due to the applied magnetic field (a result of hysteresis), and also due to handling, mounting, and loading of the annealed shield. Disassembling-assembling a shield [31] can increase the residual magnetization of the innermost layer leading to an increase of the residual magnetic field in the shielded volume up to 300 μG, compared to the typical value after degaussing of 10 to 50 μG.

In order to increase the effective permeability and decrease the residual magnetic field inside the shield, a special procedure known as demagnetizing (degaussing) is used. Degaussing consists in applying to the shielding material a slowly decaying alternating magnetic field. The maximum value of the applied field should produce a field in the material enough for its complete saturation. Reference [47] recommends the maximum demagnetizing field to be five times the material coercivity H_c, which is specified to be $H_c = 15$ mOe for CO-NETIC AA [46]. After such treatment, the magnetization properties of the ferromagnetic material are described with an anhysteretic magnetization curve (Fig. 12.3) and corresponding anhysteretic (ideal) permeability μ_{an} (see, for example, Refs. [43, 45, 38]), which can significantly exceed μ_{in} [48].

It should be emphasized that demagnetizing improves the shielding performance only for purely static fields by generating the magnetization of the shield that compensates an applied field and results in a lower field inside the shield. For shielding of the varying part of the external field after demagnetizing, μ_{in} is still appropriate. The relation between the demagnetizing field and anhysteretic magnetization is the subject of investigation in Ref. [49]. Demagnetizing is usually used to bring the shield into ideal conditions at its installation and periodically during its operation.

However, the advantage of the large anhysteretic permeability can also be used for shielding of slowly varying fields if a demagnetizing (*shaking*) oscillating field is steadily applied. This type of operation can yield much better shielding efficiency [50, 51]; see also a dedicated subsection below.

Usually demagnetizing is accomplished by winding a special coil around a shielding shell (in solenoidal and/or toroidal configuration) and supplying the coil with ac current at an industrial frequency of 50 or 60 Hz [48, 52, 53, 54]. The demagnetizing current is gradually reduced from a large (material-saturating) value to zero, for example, by means of a variable autotransformer as it was done in Ref. [53]. For a smooth change of the current, a current-control system based on an induction variometer (variocoupler) was developed in Ref. [54]. It ensures a smooth decrease in the demagnetization current by a factor of 10^3 without sudden variations, which arise as the autotransformer runner jumps from one turn of its coil to another.

Another demagnetization arrangement is used in Refs. [17, 55, 56, 57]. A current is passed through the center of the shields using either an existing vacuum can as a conductor [17, 56, 57] or a dedicated wire on the axis of the shields [55]. Due to ineffective single-turn-coil geometry, the demagnetizing current has to be large, up to 3 kA at 50 Hz, requiring a rather complicated current control system [57].

Note that demagnetization of a ferromagnetic material can be achieved by applying a static magnetic field, oppositely directed with respect to the residual magnetization. After the applied magnetic field is removed, the magnetization is restored only partially. By 'overshooting' the applied field, it is possible to achieve nearly complete demagnetization. Static-field demagnetization of a ferromagnetic shield was used by Zolotorev [58] in order to locally zero the residual magnetization over the 'bad' spots of a shield.

Mechanical shaking and tapping

Understanding the effects of mechanical treatment of a ferromagnetic shield is not straightforward. The handling and mounting of an annealed shield, as well as the loading stresses, shock, vibration, and applied magnetic fields is known to cause degradation of the permeability and the residual magnetization. For example, in Refs. [25, 47] a decrease of the permeability by a factor of two and even more was observed. In contrast to this observation, shaking and vibrating a ferromagnetic shield can also result in partial demagnetization, similar to the effect of degaussing with an oscillating magnetic field [47]. Accordingly, a number of researchers have observed that gentle tapping on the shield can help the degaussing process to lower the residual magnetization of the shield [59]. The same mechanical factors can also increase the residual magnetic field noise in the shielded volume.

In soft ferromagnetic materials placed in a low magnetic field with a strength near that of the coercive field, the magnetization process is mainly due to domain wall motion [38]. Interaction of the motion with the disorder present in the material due to impurities, lattice dislocations, residual stresses, etc., leads to sudden

changes (jumps) of the magnetization. These jumps are known as the Barkhausen effect [60]. The Barkhausen effect plays a fundamental role in the demagnetization process (see, for example, Refs. [61, 62, 63]). In the application to ferromagnetic shielding practice, it is important to note that temperature variation, plastic and dynamic deformations, and ultrasonic vibration in soft ferromagnetic materials (such as Permalloy and Mumetal) strongly affect the Barkhausen effect [64, 65, 62].

Shaking

Increasing effective permeability of a ferromagnetic shield material by shaking (that is by applying an alternating magnetic field directed to circulate along the shielding layer) was first implemented in Refs. [50] and [51]. With a large enough amplitude of the shaking field and at a frequency several times higher than the frequency of the varying outside magnetic field, the average magnetization of the shielding material follows the anhysteretic magnetization curve (Fig. 12.3). The resulting effective permeability appears to be significantly larger than the initial permeability of the shielding material. For effective shaking, the rms amplitude of the applied field should be on the order of the coercivity that is about $0.02-0.05$ Oe for magnetically soft materials (see, e.g., Refs. [38, 48, 51, 52]).

The improvement of the shielding efficiency due to shaking depends on shielding design, arrangement, and environmental conditions. In Ref. [52] with a single-layer rectangular shield biased by the Earth's magnetic field, shaking at 50 Hz increases the shielding efficiency by a factor of five. An increase by a factor of eight has been reported for a two-layer shield [51].

While implementing shaking, it is necessary to take care of possible leakage of the shaking field into the shielded volume [52, 66, 67, 68, 69]. The problem of the leakage field can be overcome if shaking is applied only to the outer shells; then the innermost layer shields the leakage field, as implemented, e.g., in Refs. [66, 54, 70]. However, this approach leads to a low efficiency of shaking. For the case of a cubic magnetically shielded room with three nested cubic shells [66], shaking applied to two outer shells improves the shielding only by a factor of 2.

An interesting approach to avoid leakage of the shaking field was used in Ref. [57]. In this set-up, a five-layer shield suppresses magnetic field inside a vacuum system placed inside the shield and consisting of a hollow cylindrical vacuum chamber with axial input and output tubes. The vacuum system is used as a conductor for an alternating current ($1-3$ A) that induces a shaking field in the innermost shell. The returned current is passed through the outside shield case. In this arrangement, shaking improves transverse field shielding by a factor of approximately 10 and the longitudinal one by a factor of ~ 7, without leakage of the shaking field.

12.2.4 Magnetic-field noise in ferromagnetic shielding

Even with perfect shielding of external magnetic fields, modern precision measurements can be limited by magnetic field noise at the level of $1 - 10 \times 10^{-11}$ G/$\sqrt{\text{Hz}}$ caused by thermal fluctuation of magnetic domains (magnetization fluctuation, see Sec. 12.3.3) and thermal agitation of conduction electrons (Johnson-Nyquist thermal currents) in the innermost layer of the magnetic shield itself [71, 72, 33, 73]. Superconducting magnetic shields (see Sec. 12.4) do not generate magnetic noise, but thermal radiation shields, required for their use with room-temperature samples, typically generate magnetic noise at a $1 - 3 \times 10^{-11}$ G/$\sqrt{\text{Hz}}$ level [74]. For comparison, the thermal magnetic noise from a human body is much lower, approximately 10^{-12} G/$\sqrt{\text{Hz}}$ [75].

A comprehensive analysis of the magnetic field noise from high-permeability magnetic shields with different geometry is presented in Ref. [73] based on the fluctuation-dissipation theorem. A back-of-the-envelope consideration of magnetic field fluctuations due to Johnson-Nyquist thermal currents and a thorough discussion of the practical consequences for high precision measurements can be found in Ref. [76].

For a large, thin metal sheet of resistivity ρ at finite temperature T, the rms magnitude of the magnetic induction $\langle B^2 \rangle$ at a distance a from the sheet is given (in quasistatic approximation) by (see, for example, Ref. [76])

$$\langle B^2 \rangle \propto \frac{4 k_B T \Delta f \delta}{c^2 \rho a^2} \ , \tag{12.10}$$

where k_B is the Boltzmann constant, c is the speed of light in vacuum, Δf is the measurement bandwidth, and δ is the sheet thickness. Equation (12.10) directly follows from the Nyquist theorem for voltage noise across a resistor (see, for example, Ref. [77]).

The magnetic field noise (Eq. 12.10) found in the quasistatic approximation is independent of frequency (white noise). However at high frequencies, currents induced in the metal by a changing thermal magnetic field and the magnetic field induced by these currents are not negligible. The induced currents tend to significantly reduce magnetic field fluctuations (self-shielding effect) at frequencies above the cut-off frequency f^* given by [76]

$$f^* \propto \frac{c^2 \rho}{2\pi \delta a}. \tag{12.11}$$

Magnetic field noise inside a shield can be significantly diminished by carefully designing the shell structure of the shield. According to Eq. (12.10), the thickness of the innermost layer should be as small as possible. However, it would lead to a proportional increase of the cut-off frequency, and, therefore, to a relative gain of magnetic noise at high frequencies. An increase of distance a (and, accordingly, an innermost layer size) is beneficial for the decrease of both, the noise level and

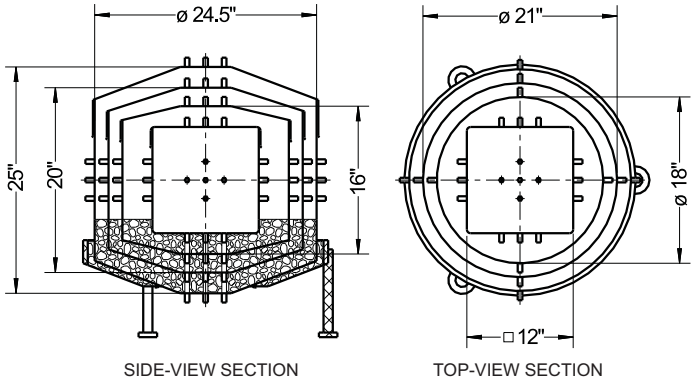

Figure 12.4
Geometrical configuration of the four-layer magnetic shield at Berkeley [31].

the cut-off frequency. Another effective way is to use an innermost layer made of a material with low electrical conductivity, such as ferrite (see Sec. 12.3).

When designing a shield, the reflection effect should also be taken into account. As pointed out in Refs. [71] and [78] a Mumetal plate behind a good conductor plate amplifies the thermal magnetic noise. The noise of the conductor plate is suppressed if the order of the plates is changed.

Note that the detected noise level depends on the magnetic field sensor and the method of detection. The noise detected by a finite-size sensor decreases, relative to that measured by an infinitely-small sensor, with increasing the distance to a conducting plate. Use of gradiometric measurements also enables reduction of the detected magnetic field noise by an order of magnitude [71].

12.2.5 Examples of ferromagnetic shielding systems

The Yashchuk et al. Shielding System

The configuration of a four-layer ferromagnetic shielding system developed at Berkeley [31] for investigation of nonlinear magneto-optical effects with alkali vapor cells [79] is shown in Fig. 12.4.

In the design shown in Fig. 12.4, for the three outer layers employ an approximation to a spherical shape, simpler to manufacture than a true sphere. The innermost shield is in the shape of a cube with rounded edges. This allows compensation of the residual magnetic field and its gradients as well as application of relatively homogeneous fields with a system of nested 3D coils of cubic shape. The field homogeneity is increased by image currents, due to the boundary conditions at the interface of the high-permeability material, which make the short coils into effectively infinite solenoidal windings.

The layers are spaced with polyurethane foam to reduce mechanical stress. All CONETIC parts (0.4 mm thick) were annealed in a hydrogen atmosphere upon manufacturing. For demagnetization, a degaussing AC current with the maximum

amplitude of 2 A is applied to the inner coils. The shield is designed to allow optical access through a number of 1/2-in diameter holes. Each of the holes has an associated 1-in stem preserving the shielding properties.

Note that variation of the laboratory magnetic field due to motion of an elevator (about 10 m from the lab) is up to 5 mG. Variation due to the Sun's magnetic activity, measured during a magnetic field storm, reaches 30 mG. Fields of such values are monitored with a fluxgate magnetometer. The signal from a fluxgate magnetometer is used to partially compensate and stabilize the lab's magnetic field via a feedback-loop system consisting of a 3D set of relatively large outside coils and a current amplifier.

The careful design of the Berkeley magnetic shielding system allows for an overall shielding efficiency of $\sim 10^{-6}$ (roughly the same in all directions) and a long-term magnetic-field stability inside the innermost shield at the level of 0.1 μG. Five-layer versions of this basic design have demonstrated passive shielding ratios of better than 10^{-7} [80].

Magnetically shielded rooms

An ultimate approach to magnetic shielding for biomedical measurements is the employment of magnetically shielded rooms (MSRs) accommodating both a subject and the measurement equipment. An MSR is used to create a wide measuring space with a residual magnetic noise at a level of several fT/$\sqrt{\text{Hz}}$ in a magnetically and vibrationally hostile city environment.

A typical MSR [81, 82, 83, 84, 85, 86, 87, 88, 89, 47] consists of three to eight nested layers made of a few millimeter thick, high permeability ferromagnetic plates. At least one electromagnetic shielding layer, which is important at frequencies above 1 Hz, is also included. This layer is usually made of about 10 mm thick aluminum plates. Electric and magnetic continuities of the conductive and magnetic layers are maintained by overlay strips. The junctions in the aluminum layer can be electroplated with silver or gold to further improve the conductivity [81].

Commercially available MSRs [82] with three layers (Permalloy, Aluminum, Permalloy) have a 12 m^2 floor space, about 0.5 m wall thickness, weigh 6.8 tons, and provide a shielding field attenuation of about 40, 60, and 100 dB at 0.01, 1, and 100 Hz, respectively.

An extraordinary MSR is described in Ref. [83]. It has inside and outside sizes of a 2.9 and 6 m cube and comprises seven layers of Mumetal, with a 27 mm total thickness, and an aluminum layer. The MSR provides field attenuation of about 97, 153, and 166 dB at 0.01, 1, and 5 Hz, respectively.

12.3 Ferrite Shields

Ferrites are metal oxides with ferrimagnetic order. Ferrites with low coercivity, or soft ferrites, are widely used for high-permeability, low-loss magnetic components in radio-frequency, microwave, and power electronics. The primary advantage of ferrites in these applications is low electromagnetic power loss due to low electrical conductivity. At 100 kHz, for example, a typical manganese-zinc ferrite has an electrical conductivity 6–8 orders of magnitude lower than that of silicon-iron, which leads to reduction in eddy-current losses by the same factor.

Given the intimate relationship between eddy current loss and Johnson-Nyquist noise, it is no surprise that ferrites make an excellent candidate for low-noise magnetic components in compact magnetometers. Room-temperature magnetic shields and a flux concentrator made of soft ferrites were recently demonstrated [33, 90, 91]. As atomic magnetometers become increasingly more sensitive, the possibility of creating a subfemtotesla magnetic-field environment with a non-metallic magnetic shield has gained much interest. In this section we survey properties of ferrites as they pertain to the design and construction of a magnetic shield for table-top experiments.

12.3.1 Permeability

Two important classes of soft ferrites are manganese-zinc (MnZn) and nickel-zinc (NiZn) ferrites. The former has higher permeability, whereas the latter has better high-frequency loss properties. The initial permeability of MnZn ferrites ranges from several hundred to several thousand. This is smaller than the permeability of Mumetal. In order to obtain a high shielding factor, therefore, it is preferable to use ferrite in the innermost layer of a multi-layer magnetic shield, in which the outer layers are made of conventional magnetic metal. Thermal magnetic noise of the latter is then shielded by the ferrite inner layer.

The permeability of ferrites varies significantly with temperature. Two temperatures of interest are the compensation temperature, T_{comp}, and the Curie temperature, T_{curie}. At $T = T_{comp}$ the magneto-crystalline anisotropy, which is the energy barrier for domain rotation, is minimized and permeability thereby increased. Ferrito para-magnetic phase transition occurs at T_{curie}, with accompanying rise and collapse of magnetic susceptibility. Many commercial-brand soft ferrites are engineered in chemical composition to allow maximum permeability or minimum temperature coefficient around room temperature. Variation of permeability by as much as 50% is common in MnZn ferrites in the temperature range of 0 to 100°C. For an extensive review of temperature dependence of permeability and other properties of soft ferrites see Ref. [92].

12.3.2 Fabrication and the effect of an air gap

Like any ceramic materials, ferrites are brittle and cannot be readily formed into sheets, tapes, and other low-dimensional or complex shapes. This makes construction of a large magnetic shield (such as MSR) entirely out of ferrite very costly and perhaps impractical. At Princeton a cylindrical enclosure has been constructed [33] with the inner volume measuring 10 cm (height)× 10 cm (diameter), out of three — one for sidewall and two for endcaps — MnZn ferrite pieces. The sidewall piece, a hollow cylinder with 1 cm wall thickness, was formed by machining from a solid cylindrical block of ferrite, fabricated by powder mixing and sintering [93].

As ferrite shields are assembled from multiple parts, low-permeability (air or glue) gaps are introduced due to surface roughness and unevenness. According to magnetic-circuit theory (Sec. 12.2.1), an air gap inserted in a high-permeability magnetic medium behaves like a low-conductivity gap inserted into a current-carrying wire. If the gap length is X_g and the length of the path through the ferrite is X, the total magnetic resistance is

$$R_m = \sum \frac{X}{\mu S} = \frac{X_g}{1 \cdot S_g} + \frac{X}{\mu_{ferr} \cdot S} \approx \frac{1}{\mu_{ferr} S} \left(\mu_{ferr} X_g + X\right) \ , \tag{12.12}$$

where μ_{ferr} is the relative permeability of the ferrite, and we assumed that the cross sectional areas of the flux path in the air gap (S_g) and in the ferrite (S) are approximately the same. We see that the gap effectively increases the magnetic length of a flux path by $\mu_{ferr} X_g$. Therefore, for an air gap not to affect the shielding factor significantly, the gap length should be small compared to the original path length in the ferrite divided by μ_{ferr}. For $X = 10$ cm, $\mu_{ferr} = 5000$, X_g should be much less than 20 μm. Modern grinding and lapping techniques allow preparation of a sizeable ferrite block with surface flatness within a few microns.

12.3.3 Thermal noise

Thermal fluctuations of magnetic domains produce magnetic field noise inside a ferrite shield with power spectral density rising as $1/f$ with decreasing frequency. Quantitative evaluation of magnetic field noise emanating from a linear passive medium can most easily be done by invoking the generalized Nyquist relationship, also known as the fluctuation-dissipation theorem. In this approach, the problem of calculating equilibrium magnetic-field noise is conveniently replaced by that of energy-loss calculation in a driven medium. A number of commercial finite element analysis packages (e.g. Ansys Maxwell or Comsol Multiphysics) allow calculation of electromagnetic power loss in an arbitrarily shaped magnetic shield in three dimensions. The shield is harmonically driven by a point dipole or a small test coil located where magnetic field noise is to be calculated. The power loss is converted

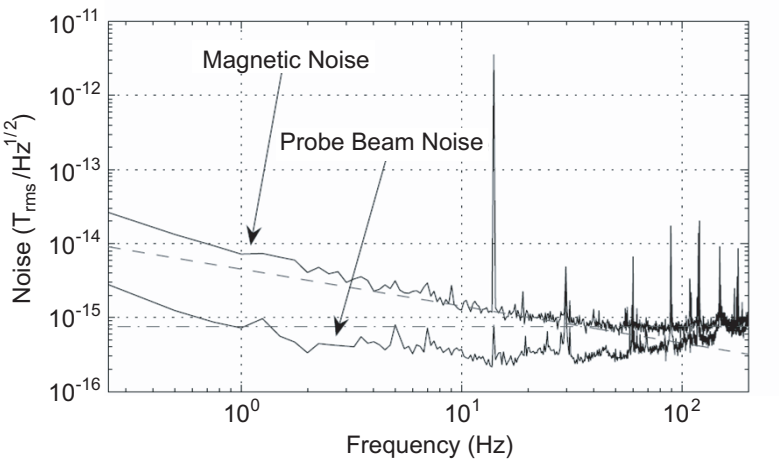

Figure 12.5 Magnetic-field noise from the Princeton ferrite shield [33]. The dashed line represents noise of 4.4 $f^{-1/2}$ fT where f is in Hz. In comparison, white noise from a Mumetal shield of the same size was estimated to be 18 fT/$Hz^{1/2}$.

to the magnetic-field noise by

$$S_B(f) = \frac{2kTP(f)}{\pi^2 p^2 f^2} \ . \tag{12.13}$$

Here, $S_B(f)$ is the power spectral density of the magnetic field noise at frequency f, kT is the thermal energy at temperature T, p is the amplitude of the driving dipole moment, and $P(f)$ is the power loss spectrum.

For metallic shields, $P(f)$ is almost completely dominated by the eddy current loss, $P(f) \propto f^2$, which gives rise to a frequency-independent (white) magnetic field noise attributable to fluctuating electric currents. On the other hand, energy loss associated with magnetic viscosity, or hysteresis loss[1], exhibits a frequency spectrum $P(f) \propto f$. The resulting $1/f$ noise has been observed in inductor cores, ferrite magnetic shields [33], and flux concentrators [90].

Analytical calculation of the magnetic-field noise in a cylindrically symmetric shield [73] has shown that as the frequency lowers, the $1/f$ noise surpasses the white noise when the skin depth of the shield becomes comparable to the thickness of the shield divided by the square root of the magnetic loss tangent, $\tan\delta_{loss}$. For 1 mm-thick Mumetal, the crossover frequency is estimated to be about 0.1 Hz, whereas for a 1-cm thick MnZn ferrite, it is on the order of 1 kHz.

For a cylindrically symmetric geometry, the magnetic-field noise due to eddy-

[1] We refer to magnetic energy loss in the limit of vanishing driving field, which in ferrite literature is distinguished from high power hysteresis loss and is often called "residual loss".

current loss is given by

$$\sqrt{S_B(f)} = \frac{G\sqrt{kT\sigma t}}{a} \ , \tag{12.14}$$

where G is a dimensionless geometrical factor of order unity, a is the linear dimension of the shield, and t and σ are its thickness and conductivity, respectively. The corresponding formula for the $1/f$ noise is

$$\sqrt{S'_B(f)} = \frac{\sqrt{kT \tan\delta_{loss}/\mu_r}}{a\sqrt{\omega t}} G' \ , \tag{12.15}$$

where the magnetic loss factor $\tan\delta_{loss}/\mu_r$ has replaced the electrical conductivity, and the thickness term appears in the denominator. The latter is valid as long as t is sufficiently large to ensure that the ferrite enclosure has a shielding factor much greater than unity.

Equation (12.14) indicates that the white noise of MnZn ferrite with its low conductivity should be ~ 3 orders of magnitude smaller than that of a ferromagnetic shield, even if the latter is much thinner (for example, 1 mm vs 1 cm). Despite the rise of the magnetic-domain noise at low frequencies, ferrite shields still show 1 – 2 orders of magnitude less noise than a ferromagnetic shield in the frequency range of 10 – 100 Hz (Fig. 12.5).

Commercial-brand soft ferrites are typically optimized for loss at radio frequencies and loss factors below 1 kHz are poorly documented. Laboratory tests on several MnZn ferrite samples from different manufacturers indicate that the lowest loss factor in the zero-frequency limit is in the range of $\tan\delta_{loss}/\mu_r = 10^{-7}$–$10^{-6}$. It may be possible that customized process optimization could further bring down the low-frequency loss factor while maintaining high permeability.

12.4 Superconducting Shields

The use of a superconducting magnetic shield in atomic magnetometry was reported as early as in 1976 [94]. In SQUID (superconducting quantum interference device) magnetometry, on the other hand, it is customary to have a SQUID chip inside a superconducting Nb shield and couple magnetic field signals originating from the outside of the shield to the sensor via a superconducting flux transformer. Because of the high cost of large-scale cryogenic cooling, superconducting shields are often designed to provide shielding over a relatively small volume, say, of 1 liter of less. Resulting proximity of the shield to the magnetometer generally raises two questions — noise and back action. In the case of a superconducting shield, the Johnson-Nyquist noise current from unpaired electrons [94] is many orders of magnitude lower than the Johnson-Nyquist noise in a metallic shield. Low temperature of the shield also means that any thermal noise from a given loss mechanism is suppressed

accordingly. Often a bigger concern with a superconducting shield in terms of noise is trapped magnetic flux in the imperfections of the material or holes in the shield, which can drift over time and is hard to control over repeated cool-down cycles. The issue of back action of the shield is discussed at the end of this section.

12.4.1 Principles

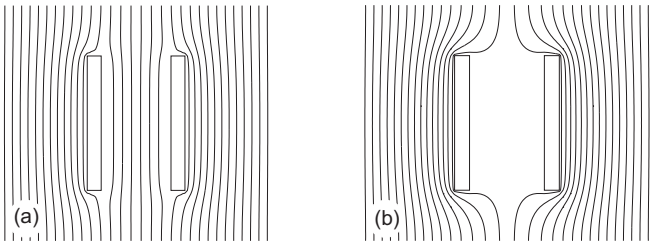

Figure 12.6 Magnetic field lines around an open superconducting cylinder. (a) Field was applied before the cylinder became superconducting. (b) Field was applied after the superconducting transition.

Magnetic field repulsion or perfect diamagnetism is a defining property of a superconductor. Magnetostatics involving a simply connected superconducting material can be modeled by assigning the latter a vanishing relative permeability, $\mu_r = 0$. In the magnetic circuit analogy, such material represents a magnetic insulator, $X/(\mu t) = \infty$. For a multiply connected superconducting piece, such as an enclosure with holes, proper modeling requires additional consideration, namely flux conservation in a superconducting ring [95]. Flux conservation makes the magnetic field distribution inside a multiply connected shield dependent on the history of the shield. Figure 12.6 shows magnetic field lines around a hollow cylinder to which an external magnetic field was applied before (a) and after (b) the superconducting transition occurred. Note that in case (a), the field inside the cylinder is even slightly increased due to the superconductor (flux focusing). In order to create a zero-field shielded region, therefore, it is important to cool down a superconducting shield itself in a (temporary) zero-field environment. A conventional ferromagnetic shield is often used for such a purpose.

Zero-field cooldown is less critical for shielding against a time-dependent magnetic field. However, it is still beneficial because flux trapped in the shield can cause field drift inside the shield due to temperature changes, thermal activation, and mechanical vibration. Removal of trapped flux after cooldown is considered practically difficult, although a method was discussed in Ref. [96].

Completely closed superconducting enclosures have an infinitely high shielding efficiency. The effect of a hole is comparable to that in a high-permeability shield. The magnetic field inside an open cylindrical superconducting shield falls off with

distance x from the opening as Eq. (12.9), with $\beta = 7.66$ and 3.68 for an axial and transverse applied field, respectively [97].

12.4.2 Materials and fabrication

A small-volume superconducting magnetic shield operating at the liquid- helium temperature can readily be assembled from machined lead blocks and rolled lead sheets. The lead parts can be joined together with conventional Pb-Sn solder, which becomes superconducting at around 7 K. For example, a closed-bottom, open-top lead cylinder with 7.5 cm diameter and 40 cm height can be constructed entirely by soldering along the seam of the sidewall and around the bottom cap. A shielding efficiency in excess of $10,000$ can be achieved in a shield made in this fashion.

The shielding efficiency can be further enhanced by nesting multiple layers of superconducting shield. As an early example, a three-layer, open-top cylindrical lead shield with inside dimensions of 51 cm (length) and 12 cm (diameter) was reported to have achieved a shielding efficiency of 10^6, limited by trapped magnetic field in the walls of the shield [98]. In this example, each lead layer had a hemispherical bottom formed by mold casting and cold pressing. The hemispherical shape helped expel the earth's magnetic field effectively from the central axis of the shield radially to the outside of it as the shield was immersed in liquid helium in an upright position.

A lighter and more mechanically reliable shield can be constructed from Nb and Nb alloys. A 1 cm-diameter Nb-Zr alloy tube often houses a SQUID and other superconducting components in SQUID magnetometry. Both Nb and Nb alloys are machineable with conventional shop tools. Nb parts can also be welded together in an argon environment. Due to the high cost of material and custom fabrication, solid monolithic Nb shields have been primarily limited to compact-sensor applications, encompassing a volume of no more than several cubic centimeters. An interesting recent development is electrolytic coating of Nb and Nb alloys on a normal conducting substrate. A spherical superconducting shield was fabricated this way to achieve an isotropic shielding efficiency of 10^7 [99].

Magnetic shields have also been made from high transition temperature superconducting materials for operation at temperatures substantially higher than 4 K. A BSCCO (bismuth strontium calcium copper oxide) superconducting shield has been demonstrated for biomagnetic measurements using SQUIDs [100]. The shield was cooled down by circulating cold helium gas and was large enough to accommodate a human subject for magnetoencephalography (MEG) studies. Magnetic-field noise was reported to be reduced by a factor of 100 at 1 Hz compared to a magnetically shielded room commonly used in MEG studies.

12.4.3 Image Field

Magnetic shields of both field absorbing and field repelling type alter the field distribution in space and therefore can affect the magnetometer measurement. For an atomic magnetometer which bases the measurement on the precession frequency of relatively concentrated magnetic moment in space, the image field from magnetic shields can affect the measurement through a shift in the precession frequency. This may be compared with the back action of magnetic shields in coil-based magnetometry, in which the presence of the shield alters the self-inductance of the coil and thereby changes calibration.

Suppose that a magnetic moment $\mathbf{p} = (p_x,\, p_y,\, p_z)$ is placed at a position $(0,\, 0,\, z)$ and an infinitely large, high-permeability plate occupies a space defined by $-h < z < 0$. The boundary condition for the magnetic field in $z > 0$ is $B_x = B_y = 0$ on $z = 0$. The magnetic field at $\mathbf{r}$ in the upper half space can be calculated by noting that the boundary condition is satisfied by an image dipole $\mathbf{q} = (-p_x,\, -p_y,\, p_z)$ placed at $(0, 0, -z)$. The field at $\mathbf{r}$ is

$$\frac{1}{(2z)^3}(p_x,\, p_y,\, 2p_z)\ . \tag{12.16}$$

The vector in the parenthesis can be decomposed as

$$(p_x,\, p_y,\, 2p_z) = (p_x,\, p_y,\, p_z) + (0,\, 0,\, p_z)\ , \tag{12.17}$$

in which the first term represents a field parallel to the dipole, and thus does not affect its precession, and the second term represents an effective static field which introduces a frequency shift of

$$\Delta\omega = \gamma\frac{p_z}{8z^3} \tag{12.18}$$

for a dipole precessing about the z axis.

A similar analysis can be followed for the reaction field from a superconducting plate. Here the boundary condition, $B_z = 0$ on the xy plane, is satisfied by an image dipole $\mathbf{q} = (p,\, p_y,\, -p_z)$ at $(0, 0, -z)$. The field at $\mathbf{r}$ is

$$\frac{1}{(2z)^3}(-p_x,\, -p_y,\, -2p_z)\ . \tag{12.19}$$

and the frequency shift is given by the negative of Eq. (12.18).

For an atomic magnetometer with cell magnetization M, the frequency shift scales as $M(R/z)^3$, where R is the linear dimension of the cell and z is the distance to the shield's wall. For a cell which is nominally spherical but possesses a small degree of non-sphericity, the residual dipolar field of the cell resulting from the non-sphericity can be comparable to the reaction field from a nearby magnetic shield. For example, a nominally spherical cell that is elongated along the z axis by 0.1% and is uniformly magnetized along the same axis would have a dipolar self field that

is 80% of the reaction field from a high permeability plate located at a distance five times the radius of the cell.

The image method can be extended to find the reaction field of magnetic shields made of multiple plates.

The dipolar reaction field inside a cubical space defined by six planes at $x = \pm a/2$, $y = \pm a/2$, $z = \pm a/2$ can be calculated by assigning image dipoles at $\mathbf{r}_{mnl} = (am, an, al)$ according to

$$\mathbf{p}_{mnl} = \left(p_x(-1)^{n+l}, p_y(-1)^{l+m}, p_z(-1)^{m+n}\right) \tag{12.20}$$

for a high permeability shield and

$$\mathbf{p}_{mnl} = \left(p_x(-1)^{m}, p_y(-1)^{n}, p_z(-1)^{l}\right) \tag{12.21}$$

for a superconducting shield. Here m, n, l are integers from $-\infty$ to $+\infty$ and $\mathbf{p} = (p_x, p_y, p_z)$ is the source dipole at the origin. The reaction field at the origin is parallel to $\mathbf{p}$ and is given by

$$\mathbf{B}_{shield,\, high\,\mu} = \frac{1}{a^3}\,\mathbf{p} \cdot 5.354 \tag{12.22}$$

and

$$\mathbf{B}_{shield,\, supercon} = \frac{1}{a^3}\,\mathbf{p} \cdot (-9.698). \tag{12.23}$$

Square and spherical shields are two examples in which the reaction field on the dipole at the center is parallel to the dipole itself, and, thus, exerts no torque on the dipole.

The dipolar reaction field of an infinitely long, cylindrical superconducting shield is calculated un Ref. [101].

References

[1] C.G. Constable, S.C. Constable, in *Frontiers and Challenges in Geophysics* (R.S.J. Sparks and C.J. Hawkesworth, American Geophysical Union, 2004), pp. 147-160.
[2] T. J. Sumner, J. M. Pendlebury, and K. F. Smith, J. Phys. D **20**, 1095 (1987).
[3] T. Rikitake, *Magnetic and Electromagnetic Shielding* (TERRAPUB and D. Reidel Publ. Co., Tokyo, Dordrecht, 1987).
[4] I. B. Khriplovich and S. K. Lamoreaux, *CP violation without strangeness: electric dipole moments of particles, atoms, and molecules* (Springer-Verlag, Berlin, New York, 1997).
[5] D. Budker, D. F. Kimball, S. M. Rochester, and V. V. Yashchuk, Phys. Rev. A **65**, 033401 (2002).
[6] K. L. Kaiser, *Electromagnetic Shielding* (Taylor and Francis, Boca Raton, 2006).
[7] J. F. Hoburg, IEEE Trans. Electromagnstic Compatibility **37**, 574 (1995).
[8] H. A. Rowland, Phil. Mag. **46**, 140(1873).

[9] A. Morley and E. Hughes, *Principles of Electricity*, 5th ed. revised by W. Bolton (Longman, London, 2007).
[10] E. Paperno and I. Sasada, IEEE Trans. Magn. (Japan) **24**, 40 (2000).
[11] I. Sasada, E. Paperno, and P. Ripka, in P. Ripka, ed., *Magnetic sensors and magnetometers* (Artech House, Boston-London, 2001).
[12] ANSYS, Inc., *ANSYS Maxwell* (http://www.ansoft.com/products/em/maxwell/).
[13] A. W. Ruker, Phil. Mag. **37**, 95 (1894).
[14] H. E. J. G. du Bois, Ann. **63**, 348 (1897).
[15] H. E. J. G. du Bois, Ann. d. Physik **65**, 1 (1898).
[16] A. P. Wills, Phys. Rev. **9**, 193 (1899).
[17] D. Kleppner, H. C. Berg, S. B. Crampton, N. F. Ramsey, R. F. C. Vessot, H. E. Peters, and J. Vanier, Phys. Rev. **138**, 972 (1965).
[18] A. J. Mager, IEEE Trans. Magn. **6**, 67 (1970).
[19] E. Paperno, H. Koide, and I. Sasada, J. Appl. Phys. **87**, 5959 (2000).
[20] E. Paperno, H. Koide, and I. Sasada, IEEE Trans. Magn. **37**, 2881 (2001).
[21] T. Rikitake, J. Geomagnetism and Geoelectricity **44**, 637 (1992).
[22] T. Rikitake, J. Geomagnetism and Geoelectricity **44**, 919 (1992).
[23] T. Rikitake, Journal of Geomagnetism and Geoelectricity **45**, 589 (1993).
[24] T. Rikitake, J. Geomagnetism and Geoelectricity **47**, 639 (1995).
[25] D. U. Gubser, S. A. Wolf, and J. E. Cox, Rev. Sci. Instrum. **50**, 751 (1979).
[26] E. Paperno, I. Sasada, and H. Naka, IEEE Trans. Magn. **35**, 3943 (1999).
[27] A. K. Thomas, EEE Trans. Electromagn. Comp. **10**, 142 (1968).
[28] E. Paperno, S. Peliwal, M. V. Romalis, and A. Plotkin, J. Appl. Phys. **97**, 10Q104 (2005).
[29] L. H. Chang, Ch. Wang, G. H. Luo, M. C. Lin, J. Magn. Magn. Mat. **239**, 591 (2002).
[30] E. Paperno, M. Romalis and Y. Noam, IEEE Trans. Magn. **40**, 2170 (2004).
[31] V. V. Yashchuk, D. Budker, and M. Zolotorev, AIP Conf. Proc. **457**, 177 (1999).
[32] A. J. Mager, IEEE Trans. Magn. **6**, 67 (1970).
[33] T. W. Kornack, S. J. Smullin, S.-K. Lee, and M. V. Romalis, App. Phys. Lett. **90**, 223501 (2007).
[34] Magnetic Shield Co., *MuMetal* (http://www.magnetic-shield.com/mumetal.html).
[35] Amuneal Manufacturing, Co., *Magnetic shielding materials* (http://-www.amuneal.com/ magnetic-shielding/theory-design/magnetic-shielding-materials).
[36] E-Song America, Inc., *Permalloy - magnetic field shielding* (http://-www.esongamerica.com/ resources/Permalloy.pdf).
[37] Magnetic Shield Co., *Sheet and Foil Material Selection Guide* (http://www.magnetic-shield.com/literature.html).
[38] R. M. Bozorth, *Ferromagnetism* (IEEE Press, Piscataway, N.J., 1993).
[39] K. Gupta, K.K. Raina, and S.K. Sinha, J. of Alloys and Compounds **429**, 357 (2007).
[40] D. J. Snee, J. Appl. Phys. **38**, 1172 (1967).
[41] W. D. Kehr, J. Appl. Phys. **41**, 1857 (1970).
[42] D. L. Martin and R. L. Snowdon, Rev. Sci. Instrum. **46**, 523 (1975).

[43] R. Boll, ed., *Soft magnetic materials: fundamentals, alloys, properties, products, applications, The Vacuumschmelze Handbook* (Heyden, London, 1979).
[44] H. Warlimont, in G. C. Hadjipanayis, ed., *Magnetic hysteresis in novel magnetic materials*, (Kluwer Academic Publishers, Dordrecht, Boston, 1997), pp. 685709.
[45] G. Bertotti, *Hysteresis in magnetism: for physicists, materials scientists, and engineers* (Academic Press, San Diego, 1998).
[46] Magnetic Shield Co., *Stress annealed CO-NETIC AA alloy* (http://www.magnetic-shield.com/products/conetic.html).
[47] E. Baum and J. Bork, J. Magn. Magn. Mat. **101**, 69 (1991).
[48] S. M. Freake and T. L. Thorp, Rev. Sci. Instrum. **42**, 1411 (1971).
[49] H. J. de Wit, J. App. Phys. **81**, 1838 (1997).
[50] T. Spooner, Phys. Rev. **25**, 527 (1925).
[51] D. Cohen, Appl. Phys. Lett. **10**, 67 (1967).
[52] V. O. Kelha, R. Peltonen, and B. Rantala, IEEE Trans. Magn. **16**, 575 (1980).
[53] E. D. Commins, S. B. Ross, D. DeMille, and B. C. Regan, Phys. Rev. A **50**, 2960 (1994).
[54] Y. V. Borisov, S. N. Ivanov, V. M. Lobashev, and Y. V. Sobolev, Nucl. Instrum. and Meth. A **357**, 115 (1995).
[55] R. Kunski and J. Vanier, J. Phys. E **15**, 1207 (1982).
[56] A. N. Kozlov, Y. V. Nikitenkio, and Y. V. Taran, Nucl. Instrum. and Meth. **192**, 379 (1982).
[57] Y. V. Taran, Instr. Exper. Techn. **27**, 1487, (1984).
[58] M. S. Zolotorev (private communications).
[59] E. B. Alexandrov, M. S. Zolotorev, S. K. Lamoreaux, and V. V. Yashchuk (private communications).
[60] H. Barkhausen, Z. Phys. **20**, 401 (1919).
[61] E. P. T. Tyndall, Phys. Rev. **24**, 439 (1924).
[62] V. M. Rudyak, Sov. Phys. Uspekhi **13**, 461 (1971).
[63] G. Durin, S. Zapperi, J. Appl. Phys. **85**, 5196 (1999).
[64] F. Forster, H. Wetzel, Zs. Metallkunde **33**, 115 (1941).
[65] H. Markert, Phys. Sta. Sol. **20**, K67-70 (1967).
[66] V. O. Kelha, J. M. Pukki, R. S. Peltonen, A. J. Penttinen, R. J. Ilmoniemi, and J. J. Heino, IEEE Trans. Magn. **18**, 260 (1982).
[67] I. Sasada, S. Kubo, and K. Harada, J. Appl. Phys. **64**, 5696 (1988).
[68] I. Sasada and Y. Ohnaka, IEEE Translation Journal on Magnetics **9**, 33 (1994).
[69] I. Sasada, E. Paperno, and H. Koide, J. Appl. Phys. **87**, 5962 (2000).
[70] I. S. Altarev, Y. V. Borisov, N. V. Borovikova, A. I. Egorov, S. N. Ivanov, E. A. Kolomensky, M. S. Lasakov, V. M. Lobashev, V. A. Nazarenko, A. N. Pirozhkov, A. P. Serebrov, Yu. V. Sobolev and E. V. Shulgina, Phys. Atom. Nucl. **59**, 1152 (1996).
[71] J. Nenonen, J. Montonen, and T. Katila, Rev. Sci. Instrum. **67**, 2397 (1996).
[72] I. K. Kominis, T. W. Kornack, J. C. Allred, and M. V. Romalis, Nature **422**, 596 (2003).
[73] S.-K. Lee, M. V. Romalis, J. Appl. Phys. **103**, 084904 (2008).
[74] L. Vanthull, R. A. Simpkins, and J. T. Harding, Phys. Lett. **24A**, 736 (1967).
[75] T. Varpula and T. Poutanen, J. Appl. Phys. **55**, 4015 (1984).

[76] D. Budker, D. F. Kimball, and D. P. DeMille, *Atomic Physics: An Exploration through Problems and Solutions*, 2nd ed. (Oxford University Press, New York, 2008), Problem 8.16, pp. 403-406.
[77] C. Kittel and H. Kroemer, *Thermal Physics*, (W. H. Freeman, San Francisco, 1980).
[78] R. Maniewski, I. Derka, T. Katila, T. Ryhanen, and M. Seppanen, Med. Biol. Eng. Comput. **23**, 9 (1985).
[79] D. Budker, V. Yashchuk, and M. Zolotorev, Phys. Rev. Lett. **81**, 5788 (1998).
[80] S. Xu, S. M. Rochester, V. V. Yashchuk, M. H. Donaldson, and D. Budker, Rev. Sci. Instrum. **77**, 083106 (2006).
[81] D. Cohen, U. Schlapfer, S. Ahlfors, M. Hamalainen and E. Halgren, in H. Nowak, ed., *Biomag 2002. Proceedings of the 13th International Conference on Biomagnetism*, (VDE Verlag, 2003).
[82] NEC TOKIN, Inc., *Product Catalog* (http://www.nec-tokin.com/english/product/pdf_dl/magnetic_shielding_chamber.pdf).
[83] J. Bork, H.-D. Hahlbohm, R. Klein, A. Schnabel, in J. Nenonen, ed., *Biomag 2000. Proceedings of the 12th International Conference on Biomagnetism*, (VDE Verlag, 2001), p.p. 970-973.
[84] A. Mager, Naturwissenschaften **69**(8), 383-8 (1982).
[85] A. Mager, in S. N. Eme, H. D. Hahlbohm, and H. Lubbing, eds., *Biomagnetism* (Berlin: Walter de Gruyter, 1981), pp. 51-78.
[86] S. Erne, H. D. Hahlbohm, H. Scheer, and Z. Trontelj, in S. N. Eme, H. D. Hahlbohm, and H. Lubbing, eds., *Biomagnetism* (Berlin: Walter de Gruyter, 1981), pp. 79-87.
[87] V. O. Kelha, in S. N. Eme, H. D. Hahlbohm, and H. Lubbing, eds., *Biomagnetism* (Berlin: Walter de Gruyter, 1981), pp. 33-50.
[88] G. Kajiwara, K. Harakawa and H. Ogata, IEEE Trans. Mag. **32**, 2582 (1996).
[89] K. Harakawa, G. Kajiwara, K. Kazami, H. Ogata, and H. Kado, IEEE Trans. Mag. **32**, 5226 (1996).
[90] W. C. Griffith, R. Jimenes-Martinez, V. Shah, S. Knappe, J. Kitching, Appl. Phys. Lett. **94**, 023502 (2009).
[91] H. B. Dang, A. C. Maloof, M. V. Romalis, Appl. Phys. Lett. **97**, 151110 (2010).
[92] E. C. Snelling, *Soft Ferrites: Properties and Applications*, 2nd ed. (Butterworths, London, 1988), Chapter 3.
[93] Ceramic Magnetics, Inc., *Mn-Zn Ferrites* (http://www.cmi-ferrite.com/).
[94] B. A. Andrianov, L. V. Sidorkina., Zh. Tekh. Fiz. **46**, 2007 (1976) [Sov. Phys. Tech. Phys. **21**, 1176 (1976)].
[95] C. Cordier, S. Flament, C. Dubuc, IEEE Trans. Appl. Supercon. **9**, 4702 (1999).
[96] J. Clem, M. M. Fang, S. L. Miller, J. E. Ostenson, Z. X. Zhao, D. K. Finnemore, Appl. Phys. Lett. **47**, 1224 (1985).
[97] J. Claycomb, J. H. Miller, Jr., Rev. Sci. Instrm. **70**, 4562 (1999).
[98] S. I. Bondarenko, V. I. Sheremet, S. S. Vinogradov, V. V. Ryabovol, Sov. Phys. Tech. Phys. **20**, 73 (1975).
[99] V. N. Kolosov, A. A. Shevyrev, Inorganic Materials, **46**, 28 (2010).
[100] H. Ohta, T. Matsui, T. Uchikawa, Neurol. Clin. Neurophysiol. **2004**, 58 (2004).
[101] H. J. M. ter Brake, *SQUID magnetometers*, PhD dissertation (Univ. Twente, the Netherlands, 1986).